Numerical simulation of film boiling heat transfer in immersion quenching process using Eulerian two-fluid approach

Cukrov, Alen; Landek, Darko; Sato, Yohei; Boras, Ivanka; Ničeno, Bojan

Case Studies in Thermal Engineering 64 (2024) 105497

Contents lists available at ScienceDirect

Case Studies in Thermal Engineering

journal homepage: www.elsevier.com/locate/csite

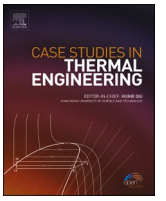

Numerical simulation of film boiling heat transfer in immersion quenching process using Eulerian two-fluid approach

Alen Cukrov [a], Darko Landek [a], Yohei Sato [b,c,*], Ivanka Boras [a], Bojan Ničeno [b]

[a] Faculty of Mechanical Engineering and Naval Architecture, University of Zagreb, Croatia
[b] Paul Scherrer Institute, Switzerland
[c] Department of Mechanical and Process Engineering, ETH Zurich, Switzerland

ARTICLE INFO

Handling Editor: Huihe Qiu

Keywords:
Immersion quenching
Two-fluid VOF
Film boiling
Remeshing
Surface partitioning

ABSTRACT

This paper presents a Computational Fluid Dynamics (CFD) simulation of the quenching process based on ISO 9950, focusing on the heat flux and heat transfer coefficient integrated over a metal specimen. The numerical method, which employs the two-fluid VOF method and frozen turbulence approach (Cukrov et al., Appl. Sci. 2023, 13, 9144), is used for the transient simulation. Since quenching processes involve complex boiling phenomena shifting from film boiling to nucleate boiling, a standard method based on VOF cannot be applied. The comparison of the simulation results with the ones obtained using correlation, and the data obtained using the Inverse Heat Transfer Analysis (IHTA) method have revealed that the proposed method can accurately predict the heat flux and heat transfer coefficient in the film boiling regime of the immersion quenching process. Note that the previous paper (Cukrov et al., Energies. 2023, 16, 7926.) presented the immersion process modeling and the temperature distribution, while the current paper examines the heat transfer characteristics of the immersion quenching process.

1. Introduction

The increased hardness obtained by martensitic microstructure is, to a first approximation, the desired mechanical property that is to be achieved via the immersion quenching process of steels. It is, however, less known that the occurrence of boiling phenomena during the process, since the initial material temperature by far exceeds the saturation temperature of the quenchant medium, is the most challenging issue in modeling such a process. The studies that encompass the macroscopic description of a multiphase flow phenomena were carried out in the past, primarily with the two methods: the mixture model and the two-fluid model (TFM). The former is, to the authors' knowledge, the first model used to estimate the transient temperature evolution in a conjugate heat transfer (CHT) simulation, which was performed by Krause et al. [1], using Lee's mass transfer model was used with a temperature-dependent empirical constant used in the selection of the appropriate boiling mode. The latter model, TFM, has recently become more widely used for flow simulations involving boiling and condensation phenomena, and the model is being continuously improved, e.g. Refs. [2–4].

A numerical method based on TFM was proposed for the simulation of a water quenching process by Srinivasan et al. [5]. The film and transition boiling regimes are taken into consideration in this model, with a constant Leidenfrost temperature as a switch criterion between the two regimes. In the film boiling regime, the heat transfer coefficient h was modeled with Bromley's correlation for a steady-state film boiling in a horizontal tube with a saturated liquid; derived analogously to Nusselt number correlation for film

* Corresponding author. Paul Scherrer Institute, Switzerland.
E-mail address: yohei.sato@psi.ch (Y. Sato).

https://doi.org/10.1016/j.csite.2024.105497
Received 22 May 2024; Received in revised form 11 November 2024; Accepted 12 November 2024
Available online 14 November 2024

condensation. Although the TFM is used, the authors formulate the energy equation for a mixture phase, alleviating the complex modeling of energy transport at the phase interfaces. The proposed model was applied to the simulation of engine cylinder head quenching by Srinivasan et al. [6]. Kopun et al. [7] extended the model of Srinivasan et al. [5] in terms of the inclusion of additional momentum transfer closures, namely lift and wall lubrication forces, and the variable Leidenfrost temperature, together with another fluid-solid energy transfer coupling interface, termed multi-material. The model was applied to the simulation of quenching of a steep aluminum plate (geometry) and an engine cylinder head. The structure of the mass transfer model is same as the base model [5], but the variable Leidenfrost temperature is introduced as a criterion for determination of the boiling regime that is present in the flow domain. In other words, in their model, the Leidenfrost temperature is used as a switch criterion between the different correlations for calculation of the interphase heat transfer coefficient which directly influences the computed mass transfer.

A numerical model for the spray quenching using the Eulerian TFM was developed by Stark and Fritsching [8]. This model can be applied not only to the film and nucleate boiling regimes that occur in the process together with the single-phase convection heat transfer, but also the condensation processes that are present in the computational domain. To accomplish this, appropriate source and sink terms were introduced to the conservation equations for mass, momentum, and energy. To determine which of the aforementioned phase change phenomena (boiling or condensation) takes place, in each computational cell two criteria are examined: the liquid temperature and the volumetric heat flow rate. First, the temperature of the liquid in the cell is compared to the saturation temperature for relevant absolute pressure in the system (hereinafter called saturation temperature). If the liquid temperature is higher than the saturation temperature (if it is lower than saturation temperature, then no mass transfer takes place, i.e., the volumetric sources are equal to zero), a limiting volumetric heat flow rate, Φ_{lim}, is computed in the cell, and compared with the cell's volumetric heat flow rate, Φ_{cell}. If $\Phi_{cell} > \Phi_{lim}$, the boiling phenomenon occurs in the domain. Otherwise, the condensation occurs. This condensation is referred to as "Condensation I", and is a consequence of the volumetric heat flow rate in the cell. Furthermore, the model considers the case when vapor temperature is lower than saturation temperature, that is, $T_v < T_{sat}$. Then, the condensation referred to as "Condensation II" takes place. This approach is implemented into ANSYS Fluent code, and has been applied to jet impingement cooling of a flat plate [8]; a conjugate heat transfer problem used to, among other results, obtain the distributions of heat transfer coefficients and surface temperatures.

Apart from TFM, the usage of the level-set method, an instantaneous interface resolving method, in conjunction with stabilized finite-element method (FEM) in the numerical modeling of the quenching process was proposed by Kosseifi [9]. The proposed model uses the variational multi-scale (VMS) approach, known also as Navier-Stokes VMS, for efficient handling of mass and momentum equations in multiphase flows with high density and viscosity ratios across the interfaces. The advection of the interface is accomplished using the sum of the growth velocity and the velocity computed as a dependent variable, that is, the transport velocity. The volume of fluid method, which is also an interface resolving method, was applied to the quenching process simulation by Moon et al. [10]. Using fine mesh, which results in small time step of the order of micro second, the computed surface temperature shows good agreement with the experimental measurement.

Going back to the TFM framework, a simulation related to jet impingement cooling of a heated surface was conducted by Subhash [11] using a different approach. The author used AVL Fire [12] code and the multi-fluid model was utilized for computation of boiling flows, that is, the quenching process. The importance of adequate modeling of turbulence in accurate estimation of wall heat transfer is emphasized, in particular the important role of turbulent kinetic energy, whilst the quenching process is modeled using the model of Srinivasan et al. [5]. A 3D industrial scale quenching model based on VMS approach, that may be regarded as a finite--element-method's mode of the large eddy simulation (LES), was proposed by Bahbah [13]. In this work, the boiling flow of a quenching process in complex geometry was demonstrated. This approach was applied to turbulent flow in conjunction with standard LES in John [14]. More recently, the fundamental issues regarding industrial scale quenching simulation were tackled by Brissot [15]. Furthermore, in a recent study by Cukrov et al. [16], the theoretical framework for modeling of turbulent flow using the so-called "frozen turbulence" approach has been proposed, and applied to a film boiling simulation around a silver specimen in a quenching process. The application of this model in a water entry, i.e., the immersion process, has been reported in Cukrov et al. [17].

Two main modeling approaches are used in quenching simulations: TFM and the interface resolving schemes such as LSM or VOF. The former approach is primarily associated with the large-scale computations and comes with the possibility to use larger time increment and coarser grids; wherein empirical closures are used in order to complete the numerical models. Here, the adaptation of empirical closures limits the generality of the model applications. In the latter approach, DNS, the liquid-gas interface is directly captured, but a sufficiently small grid size and time step are required to resolve all relevant time and length scales.

In order to avoid relying on the empirical data, as typical with the TFM model closures, but still preserving all the features of the TFM (coarse meshes and relatively large time steps), a large interface handling within the context of TFM becomes interesting to observe in this research. Thus, the identifiable interface used in single-fluid formulations, e.g. VOF, is involved in a TFM computation. To accomplish this, a two-fluid VOF method comes in handy. This kind of approach is not strange in the field of multiphase CFD modeling. Starting from, to the author's knowledge, work of Černe et al. [18] nowadays on, there were numerous attempts to combine the two approaches. Many of them were summarized in an introductory part in Mer et al. [19].

Hence, in the present study, the two-fluid VOF model available in Ansys Fluent [20] has been used in order to simulate the quenching process. The novelty of the present work is the application of two-fluid VOF method to quenching problem and the application of the model to hybrid meshes composed of both triangular and quadrilateral cells. Since the quenching process is taking place in the final stages of the steel manufacturing process, it is very important to perform it properly as it can ruin all the upstream processes and costs. By application of the two-fluid model, this may become applicable at an industrial scale, as already have been established in the field of nuclear engineering. The main difference between the quenching and nuclear application is the existence of higher heat flow rates in the case of heat treatment, and therefore making the effort for conduction of the numerical simulations more

pronounced. How this is carried out within the present research, it is explained in the remainder of the paper that is organized as follows. After this introductory chapter, the proposed numerical method is briefly described in the second chapter.

2. Numerical method

The numerical method used in this investigation is based on the Eulerian two-fluid VOF method implemented in commercial CFD software ANSYS Fluent [20], the detailed description being given in Cukrov et al. [21]. Briefly, two sets of governing equations, the conservation of mass, momentum and energy, are solved on a per phase basis, while the connection between them is established via the source terms. In this research, however, an asymptotic case of the two-fluid model is invoked by involvement of asymptotic like limits in the momentum and energy conservation equations via the anisotropic drag (momentum equations) and zero-resistance (energy equations) models. The geometrical reconstruction scheme proposed by Youngs [22] has been used in reconstruction of the interface between the phases. Since the interfacial area density is calculated as the gradient of the volume fraction, i.e., $A_{\mathrm{int}} = |\nabla \alpha_{\mathrm{v}}|$, the application of the closures in the two-fluid model can be referred to as the "locally imposed closures", because they do apply in the cells that contain the interface. This has been also found, and graphically described, in Kharangate [23]. The idea of computation of the interfacial area density using the gradient of the volume fraction has been also addressed in free surface handling in algebraic interfacial area density method (AIAD), proposed in Höhne and Vallée [24], but also the large bubble model (LBM) uses the same approach [25]. The computational domain is divided into two parts: the fluid and solid part. The computational domain and the meshes used for the simulation are depicted in Fig. 1. The computational domain is the radius of 0.1 m and the height of 1 m. The radius of the solid body is 6.25 mm and the height is 60 mm. The number of meshes for the solid domain is 8×32 in the lateral and vertical directions. The fluid domain consists of quadrilateral and triangular meshes, the number of which is 1824 and 8274 meshes respectively. The fluid mesh thickness on the solid is 0.12 mm.

The applied mesh motion algorithm involves remeshing and smoothing, and is carried out according to recommendation in Ref. [26]. The smoothing is, hence, diffusion based, wherein a diffusion equation is solved, while local cell remeshing technique is used with involved sizing function. The topological change (remeshing) has been experienced by the triangular part of the domain, due to the motion of the cylinder during the process.

The mesh sensitivity analysis was performed to verify the numerical method used in this study. The test case was the Stefan problem, which is typically used for the phase-change simulations, and the details are reported in Cukrov et al. [21]. The maximum relative error in the temperature field is shown in Fig. 2 as the function of the grid index, which is defined as $\Delta x/\Delta x_{\mathrm{min}}$. Here Δx is the grid spacing, and Δx_{min} is the minimum grid spacing used for the analysis. Three types of meshes are evaluated: uniform, stretched quadrilateral and hybrid meshes. The result of the uniform mesh features *monotonic convergence*, i.e. the error monotonically approaches to an asymptotic value as the grid spacing decreases, which is considered to be reasonable. However, the results of the other types of mesh do not feature the monotonic convergence, indicating the difficulty of the grid convergence for the two-fluid/Eulerian approach using non-uniform mesh. Pointer and Liu [27], and Gauss et al. [28] reported the irrelevance of the application of the fine mesh in the two-fluid simulation because the conservation equations are defined on a per-phase basis, while the interfacial transport is

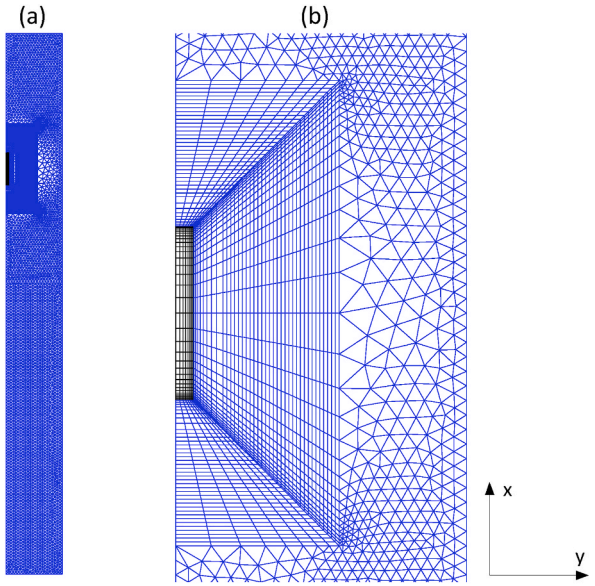

Fig. 1. The computational meshes (a) in the whole domain and (b) around the specimen in the 2D axisymmetric coordinate system. The black and blue cells represent the solid and fluid domain, respectively. The quadrilateral meshes move downward without deformation during the immersion process, while the triangular meshes are allowed to deform. (For interpretation of the references to colour in this figure legend, the reader is referred to the Web version of this article.)

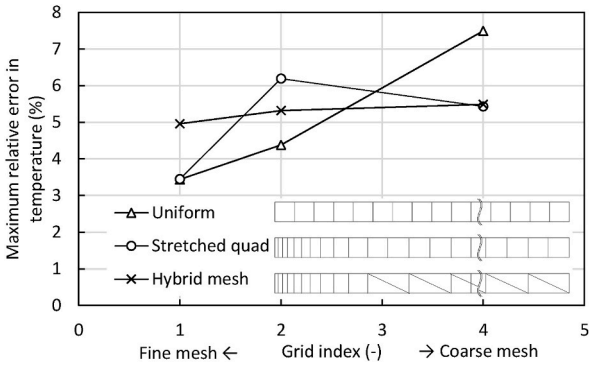

Fig. 2. Mesh sensitivity analysis of the proposed numerical method for the Stefan problem [21].

being modeled using the source terms in those equation sets. Although the mesh convergence is theoretically required for CFD simulations, the mesh convergence study for the quenching simulation is postponed to future works.

2.1. Mass transfer

The mass transfer is modeled with a novel approach, in which the mass transfer rate is calculated from the energy balance at the liquid-vapor interface. The mass transfer model has been proven to be accurate in the solution of the Stefan problem on various size and/or type grids. The idea behind this can be found in Perez-Raya and Kandlikar [29], and is compared in Fig. 3. The approach in Ref. [29] uses three probes in estimation of the distance from the so-called G-cell, the cell where from the temperature gradient is to be computed, to the interface (Fig. 3(a)). The authors claim that their approach is similar to one proposed in Sato and Ničeno [30], wherein a sharp interface calculation method for boiling flows has been proposed and validated against experimental data on nucleate boiling, and applied also in the case of film boiling that succeeded the critical heat flux in Ref. [31]. The distance d_3 is crucial in estimation of the temperature gradient. The similar approach has been used within the scope of the present research, by an assumption that the cell center distance to the interface is approximately equal to the half-width of a rectangular cell, that is, $d_3 \sim \Delta x/2$ (Fig. 3(b)).

2.2. Turbulence model

In this study, the so-called "frozen turbulence model" is used, which is described in detail in Ref. [16]. The model is a modification of the realizable k-ε model: the turbulent viscosity is a variable, but TKE is assumed to be constant. The usage of this turbulence model involves the application of the variable turbulent viscosity due to flow dependent C_μ factor. As shown in Ref. [16], the flow in the vapor phase is assumed to be laminar flow, while the turbulent flow is assumed to occur in the vicinity of the vapor-liquid interface and the bulk liquid. The jet flow is assumed to be analogous to the flow of a vapor film, and the TKE value is estimated from the Kelvin-Helmholtz instability theory [32] in conjunction with the boundary layer theory method proposed in Ref. [33].

2.3. Water entry

The downward motion of the solid sample, i.e. the immersion process, was modeled using the Arbitrary Lagrangian-Eulerian (ALE)

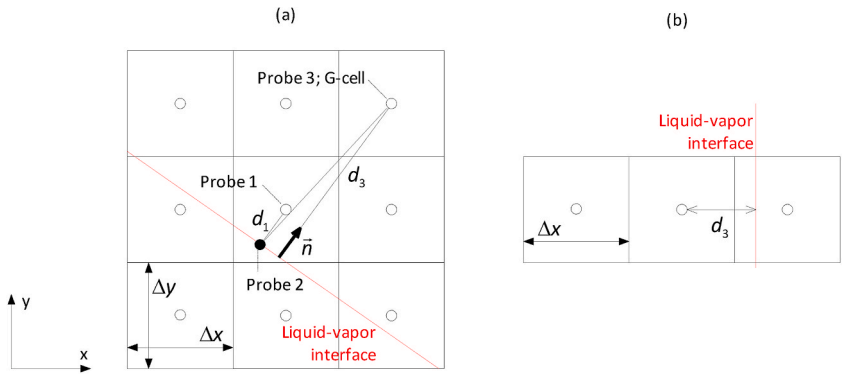

Fig. 3. The reconstruction of the temperature gradient, i.e., the calculation of the distance from the neighboring cell center to the interface: (a) the distance from the G-cell used in estimation of temperature gradient to the interface used in Perez-Raya and Kandlikar [29]; (b) the estimation of the distance in the context of the present research [21].

approach, the details of which are reported in Ref. [17]. The use of hybrid meshes (quadrilateral cells near the solid region and triangular cells in the far field) was found to be valuable in the remeshing process to cope with the topological change. The interpolation of variables was computed using Green-Gauss node-based method, due to triangular cells that are present in the domain, in conjunction with the stabilized bi-conjugate gradient stabilized method (BiCGSTAB) for solving linear system of equations, that was necessary to improve the numerical stability.

3. Studied heat transfer characteristics

3.1. Experimentally determined quantities

The experimental investigation used to validate the computational result is proposed in Ref. [34], while the one used in qualitative assessment on the temperature field transient evolution and the rewetting behavior has been already addressed in Ref. [17]. Hence, in both cases the Inconel 600 superalloy has been heated to a predefined high temperature, somewhere higher than 850 °C, in a furnace, and then is dipped down in a quiescent liquid at temperature 60 °C, as per [34], or ca. 52 °C, as in Ref. [17]. In both the cases, furthermore, the temperature is measured in the central point of the specimen, at a location 30 mm above the bottom surface of the material, using the K-type thermocouple connected with an acquisition system. The experimental setup used herein is in accordance with ISO 9950 standard. The immersion velocity is estimated as 130 mm/s [17], and this estimation is within the range of the immersion velocities applied in the experimental work in Demirel [35], that is, 100 mm/s and 200 mm/s. The estimated heat transfer coefficients in Ref. [34] are based on an inverse heat transfer (IHTA) method, that reconstructs the heat transfer coefficient values in a vicinity of a certain point of a specimen based on the previously measured temperature data. The features of the "ivfSmartQuench" system that is associated with the measurements using the ISO 9950 standard has been explained in Troell et al. [36].

3.2. Overall and partitioned heat transfer characteristics

The procedure for determination of overall heat transfer coefficient in the case of subcooled film boiling of a cylinder specimen is shown in Momoki et al. [32]. As in the case of film boiling in a liquid at saturation temperature, the calculation of heat transfer is divided into four sectors, namely: the downward facing horizontal surface (surface A); vertical surface with smooth (surface B1) and wavy interface (surface B2) between the phases; and a horizontal top surface (surface C). Thus, the overall heat transfer coefficient is again calculated using the expression for the overall heat transfer surface that has been used in the previous investigation [16], referring thereby to the aforementioned work by Momoki et al. [32]. However, it now refers to subcooled condition, since the inputs h_A, h_B and h_C now incorporate the correlations for subcooled liquid pool boiling, and are constituted from saturated part multiplied by the subcooled constant; the full description of the model equations in given in Ref. [37] (the correlations for subcooled film boiling of a finite length vertical cylinder may also be found in other publications from this group, namely Yamada et al. [38–40]).

As is the case of superheated vapor, that we had to, as in the case of Nusselt film condensation model, take the thermal properties of the unsaturated phase are for some average temperature, $\vartheta_m = (\vartheta_w + \vartheta')/2$, in the case of superheated vapor; $\vartheta_m = (\vartheta' + \vartheta_b)/2$, on the liquid side of the vapor-liquid interface. Here, ϑ_m is the average temperature used for estimation of thermal properties, ϑ_w is the wall temperature, ϑ' the saturation temperature, and ϑ_b the bulk liquid temperature. All the thermal properties were taken from Halasz et al. [41]. The material properties are listed in Table 1.

4. Results

In this chapter the experimentally obtained results are presented together with the ones obtained with the computational model presented herein. The qualitative assessments were made for the immersion quenching in case of the immersed specimen, focusing thereby on the temperature field evolution and the rewetting front behavior. Furthermore, the overall and per surface heat transfer characteristics were examined. In doing so, only the case when a body is in contact with quenchant has been considered, neglecting thereby the heat transfer to the surrounding medium prior to immersion. This is in accordance with the graphical description of the relevant specimen position for the evaluation of the heat transfer coefficient, shown in Demirel [35], and the explicit statement on the neglect of the heat transfer to the surrounding air in Li et al. [42].

The heat transfer analysis was carried out for (i) the overall surface and (ii) each of the surfaces defined in Fig. 4: the surface A (horizontal bottom), B (vertical surface) and C (horizontal top). The overall surface is the sum of the surfaces A-C. The dimensions of the specimen are defined in the ISO 9950 standard for the determination of the cooling power of liquid quenchants. The cylinder, with a diameter of $D = 12.5$ mm and a height of $H = 60$ mm, was manually immersed into a liquid bath in the experiment. The dimensions of the bath are 100 mm in diameter and 170 mm in height. The total amount of quenchant liquid is 1 l, enough to conceive the thermal

Table 1
Thermal properties of liquid water and superheated vapor phase at atmospheric pressure.

Phase	ρ, kg/m^3	c_p, kJ/(kg K)	λ, W/(m K)	μ, Pa s	Pr -
liquid, 60 °C	983.2	4.183	0.654	4.664E-4	2.981
liquid, 80 °C	971.8	4.196	0.670	3.543E-4	2.219
vapor, 477.5 °C	0.289	2.120	0.0642	2.766E-5	0.914

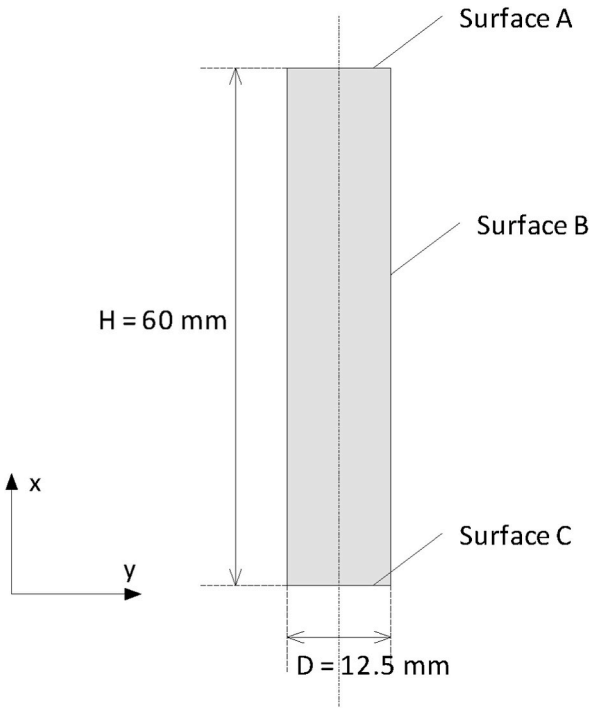

Fig. 4. The definition of the surfaces A, B and C, which are used in the partitioning of the heat transfer.

reservoir criterion by neglectable temperature change after a hot metal is immersed in the immersion quenching process.

4.1. Overall heat transfer rate

4.1.1. Qualitative assessments on the temperature field

The temperature field distribution obtained using the experiment with liquid water at ca. 52 °C, may be qualitatively tracked in Fig. 5. Since the Biot number *Bi* exceeds the lower limit of 0.1, that is known as a limiting value in the case wherein the lumped transient heat conduction model is to be applied ($Bi \rightarrow \infty$), the existence of temperature gradients with respect to space is evident thorough the process. A bottom-up temperature decrease is noted at the beginning of the cooling process.

Overall, the computed temperature distribution inside the solid material, which is shown in Fig. 6, shows similar feature to the experiment (Fig. 5), i.e. bottom-up tendency. However, there is a discrepancy in detail: the temperature at the bottom surface is apparently overestimated. We consider that the overestimation is caused by the perfectly horizontal bottom surface in the simulation. The vapor underneath the bottom surface stays there in the simulation, while the vapor may slide in the experiment due to the slight inclination of the bottom surface. These plots denote the similar tendency as the one obtained in Demirel [35] using the finite element

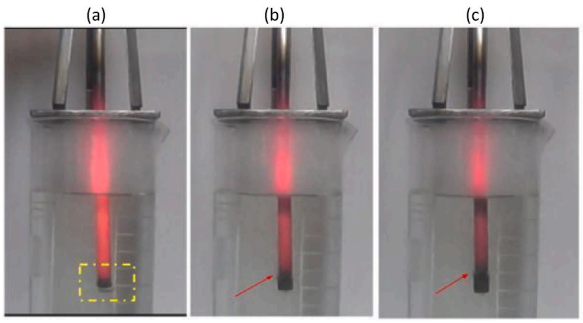

Fig. 5. The qualitative assessment of the temperature field after the immersion process: (a) the rapid decrease in temperature is present at the bottom side of the specimen, followed with the noticeable vapor zone beneath the downward facing surface (dash dot line); (b) the decrease in temperature yields the start of the rewetting front (red arrow) at the bottom part and its advancing in a bottom-up fashion; (c) the temperature around a central position of a probe showing the highest value (red zone), and the rewetting front (red arrow) advances further in the upward direction. (For interpretation of the references to colour in this figure legend, the reader is referred to the Web version of this article.)

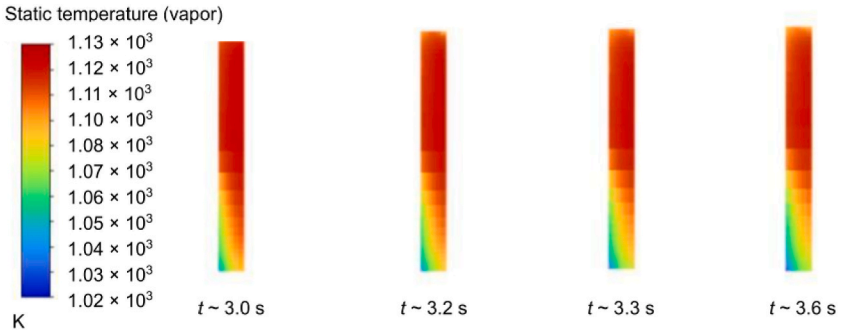

Fig. 6. The temperature distribution in a solid object during the quenching process, whilst the body remains stationary in a liquid medium.

method (FEM) in conjunction with the input data obtained from the experiment. At least when initial phases of the FEM simulation are observed. The temperature distribution, both in the experiment and the simulation, in the center of the specimen is found to experience the lowest change, that is, the temperature gradients with respect to space are the lowest in this area. This allows for, at least for some rough estimations, the application of the lumped heat conduction model ($0 < Bi < 0.1$) to estimate the cooling characteristics at this point.

By careful inspection of Fig. 5(a), one may note the mushy region beneath the downward facing horizontal surface of the specimen, denoted with the dash-dot line. It could be explained with the fact that the vapor bubble remains at the bottom of the specimen because of the horizontal bottom plane. In other words, it is the trapped vapor phase at the bottom side of the specimen which continues the film boiling mode of the heat transfer. This may be simplified as illustrated in Fig. 7(b), that can be also used to point out the boiling modes that are present in a classical immersion quenching case.

4.1.2. Quantitative analysis based on the total heat transfer coefficient and the overall heat flux

The heat transfer coefficient values presented within this section were obtained on a per surface basis, using area weighted average values extracted via the graphical user interface. The average heat transfer coefficient, compared to the data available in Landek et al. [34], obtained using IHTA agrees reasonably well. This is shown in Fig. 8.

It is noteworthy to emphasize the capturing of the vapor explosion in the simulation. This period is shown at the start of the immersion, when a body reaches free surface of the liquid water, and is followed by the increase in the integral quantities, the heat transfer coefficient and the heat flux.

The heat flux has been reported for the whole part, and it is notable that the calculated overall heat flux by means of numerical simulation agrees with the correlation result with the sufficient level of accuracy, as can be deduced from Fig. 9.

The transient oscillations are associated with the existence of dry-zones during the boiling process, as shown also in a recent study by Tecchio et al. [43]. However, due to the known difficulty to reach the transient behavior of the integral quantities (heat fluxes and heat transfer coefficients) in an experiment, for example, due to small dimensions of the specimen and extremely high temperatures that are occur during the quenching process, it is difficult to provide the comparison of our data with the experimentally obtained ones. Furthermore, IHTA modeling approach is based on previously recorded temperature data and therefrom the heat transfer coefficients are obtained, it is somehow difficult to manage the dynamics of the vapor film so precisely as with the direct approach. On the other hand, the DNS of interface motion applied to the film boiling that reported the values of the integral quantities, while computing also the temperature field within the material and the accompanied fluid flow, has not been found in the literature. Therefore, the exact

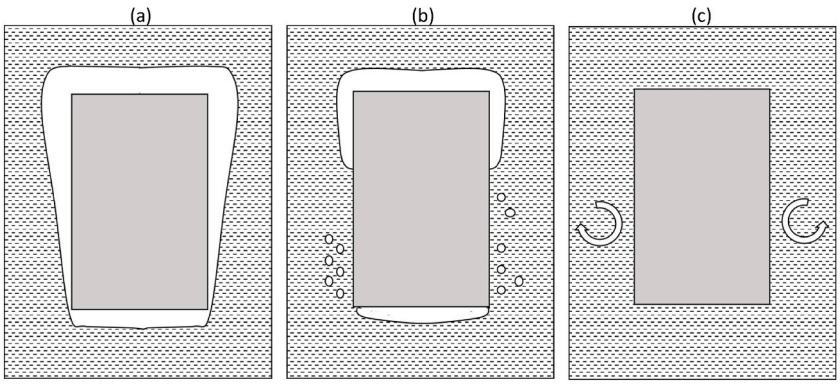

Fig. 7. A conceptual sketch of immersion quenching process: (a) film boiling mode; (b) rewetting of the specimen surface and a mushy region beneath the downward facing horizontal surface; (c) single-phase convection heat transfer - not considered within the present study.

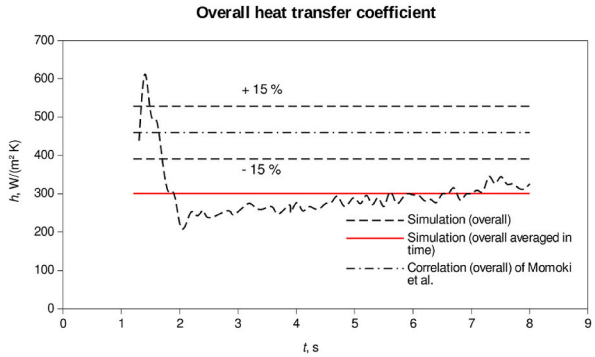

Fig. 8. Comparison of calculated heat transfer coefficients by taking into consideration all heat transfer surfaces with the results obtained using experimental data, presented in Landek et al. [34], and the correlation given in Momoki et al. [37]. The dashed lines denote ±15 % discrepancy from the correlation result.

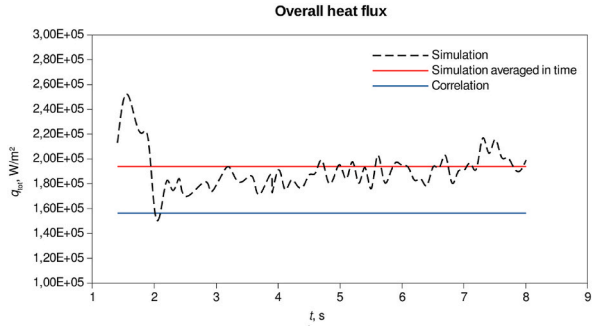

Fig. 9. The overall heat flux transferred from the solid specimen during the immersion process, after impact on a free surface level of a liquid quenchant; a comparison with the data obtained using correlations.

comparison of the transient oscillations obtained using the numerical approached applied herein with the experimental data was not manageable within the present work, due to inexistence of such data known to authors.

The heat flux partitioning has been selected in the heat transfer analysis that follows, using the surface nomenclature denoted at the beginning of this chapter.

4.2. Partitioned heat fluxes on a per surface basis

4.2.1. Heat transfer of surface A: the bottom surface

The heat transfer coefficient calculated using the empirical expressions for subcooled pool film boiling on a horizontal surface of a vertical cylinder specimen, oriented (surface, not cylinder) downward, exhibits the distribution shown in Fig. 10, and yielded the heat

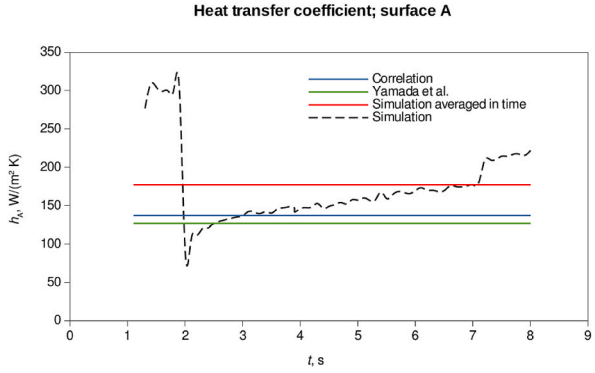

Fig. 10. Comparison of calculated heat transfer coefficients on the bottom horizontal surface by use of numerical simulation with the ones obtained with correlation available in Momoki et al. [37] and the investigation of 30 × 30 mm cylinder made of silver by Yamada et al. [39].

transfer coefficient value of 137.2 W/(m^2 K).

This is, in the same time, the first one (among the various heat transfer coefficients; namely on surfaces A, B and C) that experiences significant increase in its value as the solid body approaches the free surface of the water, i.e., the liquid medium; an order of magnitude jump of its value is noted at $t \sim 1.3$ s; from 41.16 W/(m^2 K) at $t \sim 1.2$ s up to 276.8 W/(m^2 K) at $t \sim 1.3$ s. The maximum heat transfer coefficient value is, however, slightly higher, 308.4 W/(m^2 K), at $t \sim 1.4$ s, while the minimum is reached shortly thereafter, at $t \sim 2$ s and is of value 3.4 times smaller that this, 89.5 W/(m^2 K). The average heat transfer coefficient obtained by use of numerical simulation is 177.1 W/(m^2 K).

The experimental values are taken from Yamada et al. [39], which were obtained for 500 K wall superheat on a silver cylinder with $D = L = 30$ mm, with 20 K subcooling, showing thereby the close correspondence between the simulation results and the data obtained using empirical correlations with the value of ca. 127 W/(m^2 K). Since the conditions are not perfectly matching the ones that we have in the simulation presented herein, these values are considered as the orientational ones.

The heat flux at the horizontal bottom surface, surface A, exhibits the behavior depicted in Fig. 11. This is, however, the heat transfer surface that firstly experiences the significant increase in heat flux after the material approaches free surface level of the liquid medium. This is evident in the maximum heat flux recorded in the numerical simulation at this surface that is of value 224.9 kW/m^2 at t ~1.4 s. This value corresponds to the maximum heat transfer coefficient at this surface at the same time point. The minimum heat flux value at this surface reported in the numerical simulation is 63.2 kW/m^2, and it is noticed at t ~2 s, while the average heat flux is 94.4 kW/m^2. The correlation used in prediction of the heat flux at this surface fits well with the data obtained by use of numerical simulation proposed herein, as could be drawn from the heat flux distributions. The correlation result for the heat flux at the bottom surface is 103.6 kW/m^2.

4.2.2. Heat transfer of surface B: the longitudinal surface

The dominant heat transfer surface in the model proposed in Momoki et al. [37], and Yamada et al. [39] has been divided into two parts; the smooth interface region (denoted as B1 in the model proposed by the authors), and the wavy interface region (denoted as B2 in those references). Hence, the heat transfer coefficient that embeds both regions is calculated according to definition of the heat transfer coefficient (Newton's cooling law) as:

$$\underline{h}_B = \frac{\underline{q}_B}{\Delta T_w} \tag{1}$$

where $\underline{q}_B$ (W/m^2) is the total heat flux at the vertical surface of the cylinder and ΔT_w (K) is the initial wall superheat, since both regions can be calculated with the same initial temperature differences, i.e., the wall superheats. Therefore, it is difficult to make direct comparisons with the results in Yamada et al. [39]. It could be just stated that the numerical simulation provided the values of the heat transfer coefficient within the range from 232.9 W/(m^2 K), recorded at $t \sim 2$ s and being the minimum heat transfer coefficient at this surface, to 843.8 W/(m^2 K), reported at $t \sim 1.3$ s, that is the maximum of the heat transfer coefficient recorded at this heat transfer surface and generally the highest heat flux recorded within the present study. The time averaged heat transfer coefficient of the vertical surface obtained by use of the simulation is 265 W/(m^2 K). The resulting plot is, together with simulation (instantaneous and averaged) result plotted in Fig. 12. The average heat transfer coefficient on the cylindrical surface of the Inconel 600 probe (surface B in this simulation), compared to the data available in Landek et al. [2], obtained using IHTA agrees reasonably well, as has been also shown in Fig. 12. The IHTA averaged result yields an average value of 452.8 W/(m^2 K), while the correlation results, however, is closer to the one obtained by use of numerical simulation and is 213.6 W/(m^2 K).

The heat transfer coefficient at this surface, and, therefore, the corresponding heat fluxes, that are of interest within the context of present research are those of the immersed part of the solid object. In other words, if half of the body is immersed into the liquid quenchant, then the heat transfer only of the immersed part would be considered, not a whole object's heat transfer surface. Hence, a single-phase convection heat transfer from the non-immersed part is neglected in the context of the present research, at least to a great extent, since it is somewhat difficult to sharply determine what is completely immersed due to motion of the free surface. The consideration of only the immersed part has been graphically shown in Demirel [35], whereby h $\neq$ 0 is taken inside the liquid quenching, and $h = 0$ during a single-phase convection to the ambient air.

It is, however, unphysical to consider the average heat transfer coefficients at the vertical lateral surface by taking into consideration the values from the non-immersed part. This neglect would lead to extremely high heat fluxes and corresponding heat transfer coefficients at the very beginning of the immersion process; thus yielding better agreement with the experimentally obtained data (IHTA) and the ones obtained by use of empirical correlation. The heat flux distribution with respect to time is shown in Fig. 13, and also exhibits the same tendency as the heat flux at the vertical surface of the specimen.

Thus, the maximum heat flux value recorded by use of the numerical simulation is 624.3 kW/m^2 at t ~1.3 s, while the minimum heat flux value this time does not have a correspondence with the minimum heat transfer coefficient value, since it is recorded at t ~4 s and is 167.2 kW/m^2. This non-perfect correspondence of the minimum heat flux and the minimum heat transfer coefficient may be addressed to the associated complex flow behavior that affects the temperature of the wall that appears in the denominator of the heat transfer coefficient expression.

4.2.3. Heat transfer of surface C: the top surface

It should be noted that the heat transfer coefficient at this surface shows the highest differences in the values of the extrema among the studied heat transfer surfaces, from 659.5 W/(m^2 K) at $t \sim 4$ s, as the maximum value, to 28.2 W/(m^2 K) at $t \sim 1.7$ s, being the

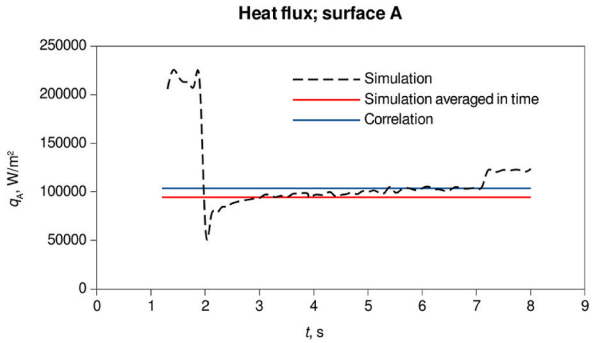

Fig. 11. The distribution of the heat flux values at horizontal bottom surface (surface A) with respect to time.

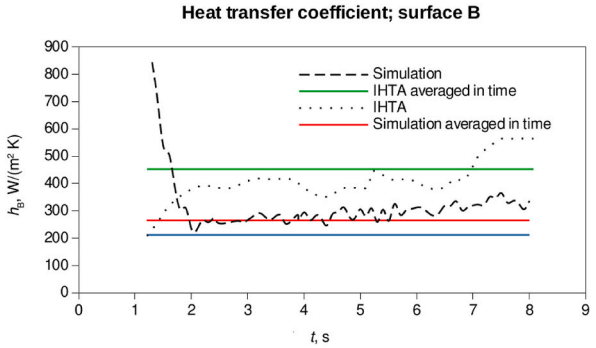

Fig. 12. Comparison of the calculated heat transfer coefficients on the vertical lateral surface with the results obtained using experimental data, presented in Landek et al. [34], and the ones obtained via the empirical correlation given in Momoki et al. [37].

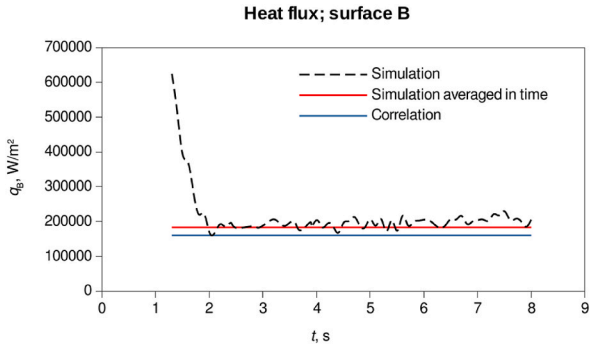

Fig. 13. The heat flux distribution versus time for vertical lateral surface; a comparison between the numerical simulation (instantaneous and the data averaged with respect to time) and the result obtained by use of correlation available in Momoki et al. [37].

minimum value, and that may be addressed to formation of a crater, that is a dry zone at the top surface of the cylinder after the cylinder is fully immersed into liquid. Furthermore, it has the lowest average value of the heat transfer coefficient, 174.1 W/(m^2 K). Fig. 14 shows good agreement between the correlation result, 184 W/(m^2 K), and the one obtained with the present model. The both results could be easily correlated to the ones obtained in Yamada et al. [39], where a result of approximately 191 W/(m^2 K) has been obtained. The similar patterns are recognizable also in the distribution of the heat flux at this surface, Fig. 15.

Since the original experiment involves a steel rod that holds the Inconel 600 probe, within this simulation it is assumed that this rod doesn't exist. Due to additional effort that has to be carried out if the steel rod is considered, for the sake of simplicity it is assumed that a free boundary is at the top horizontal surface of a cylindrical specimen.

The maximum heat flux at the top surface of the specimen is thus 463.5 kW/m^2, that is recorded at t ~4.4 s, while its minimum value is just 21.1 kW/m^2, noticed at t ~1.7 s. An average heat flux value is thus 122.3 kW/m^2, with the correlation result being close to this value, 138.9 kW/m^2.

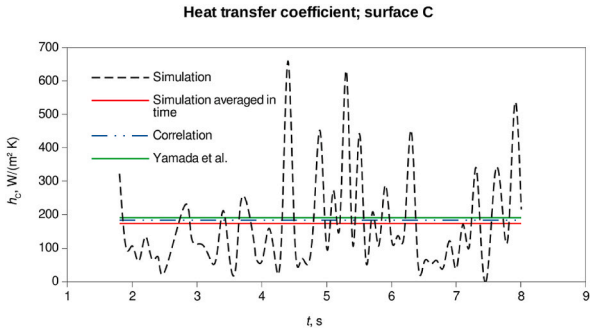

Fig. 14. The heat transfer coefficient distribution on the top horizontal surface, surface C, with respect to time together with the correlation data obtained using the model presented in Momoki et al. [37] and the data available in Yamada et al. [39].

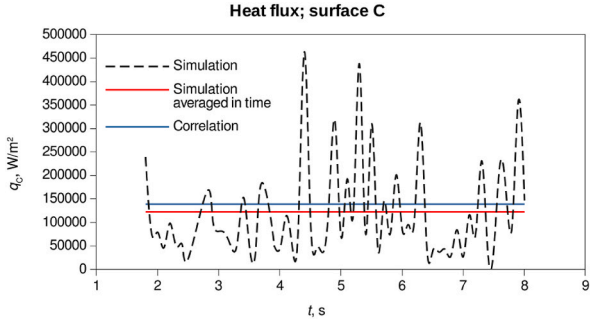

Fig. 15. The instantaneous, averaged (both simulation) and correlation obtained heat flux values at the top horizontal surface.

5. Conclusions

In this paper, a new CFD simulation method and results for the immersion quenching process have been presented. The method, based on a Eulerian two-fluid VOF formulation, can accurately predict the evolution of the temperature distribution of the solid material, under the condition of prescribed initial temperatures of the solid specimen and quenchant medium. The calculated heat transfer coefficient for the overall solid object also shows good agreement with the IHTA and the correlation result, which are consistent with each other. noting thereby that further refinement of TKE value would provide more accurate result, but, since we want, to a great extent, the model that is based on the basic principles and the derivatives thereof, fine tuning was found as an inappropriate approach in the context of the present study. The reported heat fluxes and the overall heat flux agrees relatively well with the correlation data. The graphical inspection has revealed the proper evolution of the crater, after the body is immersed into the quenchant. The reported data follows the, say, orientation, data from other investigators.

In summary, the following conclusions can be drawn from the study carried out.

1. The obtained heat transfer coefficients follow the patterns of the averaged data obtained using IHTA and the correlation ones. Although further refinement of the TKE value would yield, most probably, the more accurate result, it is claimed that it should stem from careful theoretical reasoning instead of fine tuning any simulation parameter.
2. The vapor explosion has been successfully reconstructed by use of the present numerical method, as observed from the heat fluxes and, therefore, the heat transfer coefficients, especially at the bottom horizontal surface of the cylinder that is the first one which experiences the rapid jump in these heat transfer characteristics.
3. The formation of a crater after the solid body is being completely immersed into liquid medium and its impact heat transfer have been also captured in the present simulation case; graphical inspection reveals its increased presence due to the phase change process that is present in the flow.
4. Further exploration on the partitioned heat transfer may reveal some hidden aspects of the results obtained herein; generally speaking, the heat fluxes agree reasonably well with the data obtained using correlation.

Finally, it is shown that the accepted method is suitable for film boiling simulation during the immersion quenching process in a sense that the complete heat transfer characteristics, most notably: the heat transfer coefficients and heat fluxes may be successfully tracked through the simulation. This confirms that the temperature evolution in a solid could be successfully tracked during the film boiling mode of immersion quenching process by application of the Eulerian two-fluid method, although the film boiling, due to its stratified flow nature, has been tackled primarily with single-fluid methods.

Due to the simplicity and the effectiveness of the computational model used herein, the possible further future steps are as follows:

1. Revealing the hidden aspects of the model in resolving fundamental boiling flows, such as vapor bubble rise and nucleate pool boiling.
2. Further study of turbulence modeling in the case of film boiling, aiming to the class of problems that may be accurately computed only using DNS or LES.
3. Consideration of a mixing length hypothesis (MLH) model [43], due to the observed similarity between the fully developed pipe flow with a flow inside a vapor film.
4. Replacement of the constant TKE value with an assumption of constant turbulence intensity, yielding the TKE value that would stem from the fluctuating velocity.

The other phase change simulations, such as solidification and melting, wherein the enthalpy methods are standardly used, and are usually not accompanied with a two-fluid formulation, may now be allowed to be carried out, based on the principles shown in Ref. [21].

CRediT authorship contribution statement

Alen Cukrov: Writing – original draft, Validation, Software, Methodology, Investigation. **Darko Landek:** Writing – review & editing, Supervision, Formal analysis. **Yohei Sato:** Writing – review & editing, Visualization, Supervision. **Ivanka Boras:** Writing – review & editing, Supervision, Funding acquisition, Conceptualization. **Bojan Ničeno:** Writing – original draft, Supervision, Investigation.

Declaration of competing interest

The authors declare that they have no known competing financial interests or personal relationships that could have appeared to influence the work reported in this paper.

Acknowledgements

The proposement of involvement of constant turbulence intensity instead of constant turbulent kinetic energy received by Professor Zdravko Virag, has been acknowledged. The help of Ms. Izabela Martinez in carrying out the experiment with water at ca. 50 °C, has been also gratefully acknowledged. The suggestions from Professor Emeritus Antun Galović were also sincerely acknowledged.

APPENDIX

The correlations used in the estimation of the heat transfer coefficients on a per surface basis were taken from Momoki et al. [37].

Surface A: horizontal bottom surface

The heat transfer coefficient for surface A is defined as:

$$\overline{h}_A = \left(0.699 + 0.411\ \Phi_A - 0.145\Phi_A^2 + 0.035\Phi_A^3\right)\overline{h}_{A,sat} \tag{A.1}$$

where $\Phi_A = \left[\left(\frac{J_A}{J_{A0}}\right)^3\left(\frac{1+\beta J_A}{1+\beta J_A}\right)\right]^{\frac{1}{5}}$. Here, $J_A \equiv \left(F_{A1}+\sqrt{F_{A2}}\right)^{\frac{1}{3}} + \left(F_{A1}-\sqrt{F_{A2}}\right)^{\frac{1}{3}} + \frac{1}{3\beta}\left(\frac{Sc}{Sp}\right)$

$$J_{A0} = \left(\frac{1}{2}+\sqrt{\frac{1}{4}+\frac{64}{27}\beta^3}\right)^{\frac{1}{3}} + \left(\frac{1}{2}-\sqrt{\frac{1}{4}+\frac{64}{27}\beta^3}\right)^{\frac{1}{3}};\ Sc \equiv \frac{c_{p_L}\Delta T_{sub}}{Pr_L\ r_0};\ \beta \equiv \left(\frac{R^2}{2Sp\ Pr_L}\right)^{\frac{1}{3}}$$

$$F_{A1} = \frac{1}{2}+\frac{2}{3}\left(\frac{Sc}{Sp}\right) + \left[\frac{1}{3\beta}\left(\frac{Sc}{Sp}\right)\right]^3;\ F_{A2} = \frac{1}{4}-\frac{64}{27}\beta^3 + \frac{2}{3}\left(\frac{Sc}{Sp}\right) - \frac{4}{27}\left(\frac{Sc}{Sp}\right)^2 + \left[\frac{1}{3\beta}\left(\frac{Sc}{Sp}\right)\right]^3;\ R \equiv \left(\frac{\rho_V\mu_V}{\rho_L\mu_L}\right)^{\frac{1}{2}}$$

The heat transfer coefficient in a system composed with the saturated liquid instead of the subcooled one, $\overline{h}_{A,sat}$, reads:

$$\overline{h}_{A,sat} = \overline{Nu_A}\left(\frac{k_V}{D}\right) = 1.0327\left(\frac{Gr_A}{Sp}\right)^{\frac{1}{5}}\left(\frac{k_V}{D}\right) \tag{A.2}$$

with the Grashof number $Gr_A \equiv \left(\frac{gD^3}{\nu_V^2}\right)\left[\left(\frac{\rho_L}{\rho_V}\right) - 1\right]$, and the dimensionless wall superheat $Sp \equiv \frac{c_{p_V}\ \Delta T_{sat}}{\mathrm{Pr_V}\ r_0}$.

***Surface B1*: vertical surface of the cylinder with smooth vapor-liquid interface**

The heat transfer coefficient for surface B, with smooth vapor-liquid interface, is defined as:

$$\overline{h}_{B1} = \left[1 + c_{B1}\left(\frac{Sc}{Sp}\right)\right]\overline{h}_{B1,sat} \tag{A.3}$$

where $c_{B1} = 10.45 + 11.74\frac{L}{\pi\lambda_0}$, and the capillary length λ_0 is calculated as $\lambda_0 \equiv \left[\frac{\sigma}{g\left(\rho_{L,sat}-\rho_{V,sat}\right)}\right]^{\frac{1}{2}}$ with $\rho_{L,sat}$ and $\rho_{V,sat}$ denoting the densities of saturated liquid and vapor, respectively.

The saturated film boiling heat transfer coefficient, $\overline{h}_{B1,sat}$, is defined as:

$$\overline{h}_{B1,sat} = \frac{2}{3}\left(\frac{k_V}{L_{B1}}\right)\left[(1+B)^{\frac{3}{4}} - B^{\frac{3}{4}}\right]\left(\frac{Gr_{B1}}{Sp}\right)^{\frac{1}{4}} \tag{A.4}$$

where the factor $B = 0.28228\left(\frac{D}{L_{B1}}\right)^{\frac{4}{5}}\left(\frac{Sp}{Gr_{B1}}\right)^{\frac{1}{15}}$ and the Grashof number $Gr_{B1} \equiv \left(\frac{gL_{B1}^3}{\nu_V^2}\right)\left[\left(\frac{\rho_L}{\rho_V}\right) - 1\right]$. The smooth interface length L_{B1} is defined as $L_{B1,sat} = S\,2\pi\lambda_0$, where S is an empirical factor and is taken to be 0.5 for the present research, as recommended in Momoki et al. [37].

***Surface B2*: vertical surface of a cylinder with wavy vapor-liquid interface**

The heat transfer coefficient for surface B, with wavy vapor-liquid interface, is defined as:

$$\overline{h}_{B2} = \left[1 + 0.0905\left(\frac{c_{p_V}}{c_{p_L}}\right)\left(\frac{Pr_L}{Pr_V}\right)\left(\frac{Pr_L^2}{R^2}\right)^{0.23}\left(\frac{Gr_{B_{2L}}Sp^*}{Gr_{B2,sat}}\right)^{\frac{1}{4}}\left(\frac{\lambda}{L_{B2}}\right)\left(\frac{Sc}{Sp}\right)\right]\overline{h}_{B2,sat} \tag{A.5}$$

where the corresponding Grashof number $Gr_{B2_L} \equiv \left(\frac{g\lambda^3}{\nu_L^2}\right)\left[\left(\frac{\rho_{LB}}{\rho_L}\right) - 1\right]$, and the distance of the cylinder covered with the wavy interface $L_{B2} = L - L_{B1}$. Here the L_{B1} calculated as: $L_{B1} = (1 + 56.3\,Sc)L_{B1,sat}$.

The heat transfer coefficient in the case of the saturated liquid, $\overline{h}_{B2,sat}$, is expressed as follows:

$$\overline{h}_{B2,sat} = 0.740(k_V/\lambda)\left(\frac{Gr_{B2}}{Sp^*}\right)^{\frac{1}{4}}, \tag{A.6}$$

where the dimensionless wall superheat $Sp^* = \frac{c_{p_V}\Delta T_{sat}}{\left[\mathrm{Pr}_V\left(r_0 + 0.5c_{p_V}\Delta T_{sat}\right)\right]}$, and the accompanied unit-length of a vapor film $\lambda = 16.2\left[\frac{1}{\left(Sp^{*3}\,Gr_{B_{\lambda_0}}\right)}\right]^{\frac{1}{11}}\lambda_0$.

***Surface C*: top horizontal surface of the cylinder**

The heat transfer coefficient for surface C is defined as:

$$\overline{h}_c = \left[1 + 0.0395\left(\frac{c_{p_V}}{c_{p_L}}\right)\left(\frac{k_L}{k_V}\right)\left(\frac{Sp}{Gr_{C,sat}}\right)^{\frac{1}{4}}\left(\frac{\lambda_0^3\, r_0 g\,\alpha_L Pr_L^2 Sc}{c_{p_L}\nu_L^2}\right)^{\frac{1}{3}}\left(\frac{Pr_L}{Pr_V}\right)\left(\frac{Sc}{Sp}\right)\right]\overline{h}_{C,sat} \tag{A.7}$$

with α being an isobaric volume expansion coefficient and $\overline{h}_{C,sat}$ the heat transfer coefficient at the top surface in a saturated liquid case.

The heat transfer coefficient in the case of the film boiling in a saturated liquid pool can be estimated as:

$$\overline{h}_{C,sat} \equiv \overline{Nu}_C\left(\frac{k_V}{\lambda_0}\right) = 0.425\left[\frac{Gr_C}{Sp}\right]^{\frac{1}{4}}\left(\frac{k_V}{\lambda_0}\right) \tag{A.8}$$

with the Grashof number $Gr_C = \left(\frac{g\,\lambda_0^3}{\nu_V^3}\right)\left[\left(\frac{\rho_L}{\rho_V}\right) - 1\right]$.

Data availability

Data will be made available on request.

References

[1] F. Krause, S. Schüttenberg, U. Fritsching, Modelling and simulation of flow boiling heat transfer, Int. J. Numer. Methods Heat Fluid Flow 20 (2010) 312–331, https://doi.org/10.1108/09615531011024066.

[2] R.T. Lahey, E. Baglietto, I.A. Bolotnov, Progress in multiphase computational fluid dynamics, Nucl. Eng. Des. 374 (2021) 111018, https://doi.org/10.1016/j.nucengdes.2020.111018.

[3] H. Setoodeh, W. Ding, D. Lucas, U. Hampel, Modelling and simulation of flow boiling with an Eulerian-Eulerian approach and integrated models for bubble dynamics and temperature-dependent heat partitioning, Int. J. Therm. Sci. 161 (2021) 106709, https://doi.org/10.1016/j.ijthermalsci.2020.106709.

[4] H. Wang, J. Xiong, J. Wang, Development and assessment of five-component wall boiling heat flux partitioning model, Int. J. Multiphas. Flow 158 (2023) 104306, https://doi.org/10.1016/j.ijmultiphaseflow.2022.104306.

[5] V. Srinivasan, K.-M. Moon, D. Greif, D.M. Wang, M.-h. Kim, Numerical simulation of immersion quench cooling process using an Eulerian multi-fluid approach, Appl. Therm. Eng. 30 (2010) 499–509, https://doi.org/10.1016/j.applthermaleng.2009.10.012.

[6] V. Srinivasan, K.-M. Moon, D. Greif, D.M. Wang, M.-h. Kim, Numerical simulation of immersion quenching process of an engine cylinder head, Appl. Math. Model. 34 (2010) 2111–2128, https://doi.org/10.1016/j.apm.2009.10.023.

[7] R. Kopun, L. Škerget, M. Hriberšek, D. Zhang, W. Edelbauer, Numerical investigations of quenching cooling processes for different cast aluminum parts, Strojniški Vestnik - J. Mech.Eng. 60 (2014) 10, https://doi.org/10.5545/sv-jme.2014.1705.

[8] P. Stark, U. Fritsching, Simulation of the impinging liquid jet cooling process of a flat plate, Int. J. Numer. Methods Heat Fluid Flow 25 (2015) 153–170, https://doi.org/10.1108/HFF-04-2013-0151.

[9] N. El Kosseifi, Numerical Simulation of Boiling for Industrial Quenching Processes, Ecole Nationale Supérieure des Mines de Paris, 2012. PhD thesis, https://pastel.hal.science/pastel-00734601.

[10] J.H. Moon, J. Lee, S.H. Lee, Numerical study of the boiling heat transfer characteristics of bluff body quenching in cylindrical tube, Case Stud. Therm. Eng. 32 (2022) 101900, https://doi.org/10.1016/j.csite.2022.101900.

[11] S. Maharshi, Computational modelling of liquid jet impingement onto heated surface, PhD Thesis, Technische Universität Darmstadt, http://tuprints.ulb.tu-darmstadt.de/6217/, 2017.

[12] AVL List GmbH, AVL FIRE Manual, https://www.avl.com/en/simulation-solutions/software-offering/simulation-tools-z/avl-fire-m.

[13] C. Bahbah, Advanced numerical methods for the simulation of the industrial quenching process, Université Paris sciences et lettres (2020). PhD thesis, https://pastel.hal.science/tel-03157524.

[14] V. John, A. Kindl, C. Suciu, Finite element LES and VMS methods on tetrahedral meshes, J. Comput. Appl. Math. 233 (2010) 3095–3102, https://doi.org/10.1016/j.cam.2009.06.005.

[15] C. Brissot, Numerical and experimental study of boiling flows: application to quenching, Université Paris sciences et lettres (2022). PhD thesis, https://pastel.hal.science/tel-04081852.

[16] A. Cukrov, Y. Sato, I. Boras, B. Ničeno, Film boiling around a finite size cylindrical specimen - a transient conjugate heat transfer approach, Appl. Sci. 13 (2023) 9144, https://doi.org/10.3390/app13169144.

[17] A. Cukrov, D. Landek, Y. Sato, I. Boras, B. Ničeno, Water entry of a heated axisymmetric vertical cylinder, Energies 16 (2023) 7926, https://doi.org/10.3390/en16247926.

[18] G. Černe, S. Petelin, I. Tiselj, Coupling of the interface tracking and the two-fluid models for the simulation of incompressible two-phase flow, J. Comput. Phys. 171 (2001) 776–804, https://doi.org/10.1006/jcph.2001.6810.

[19] S. Mer, O. Praud, H. Neau, N. Merigoux, J. Magnaudet, V. Roig, The emptying of a bottle as a test case for assessing interfacial momentum exchange models for Euler–Euler simulations of multi-scale gas-liquid flows, Int. J. Multiphas. Flow 106 (2018) 109–124, https://doi.org/10.1016/j.ijmultiphaseflow.2018.05.002.

[20] Ansys Inc, Ansys Fluent Theory Guide, 19.0, Release, 2019.

[21] A. Cukrov, Y. Sato, I. Boras, B. Ničeno, A solution to Stefan problem using Eulerian two-fluid VOF model, Brodogradnja 72 (2021) 141–164, https://doi.org/10.21278/brod72408.

[22] D.L. Youngs, Time-dependent multi-material flow with large fluid distortion, in: K.W. Morton, M.J. Baines (Eds.), Numerical Methods for Fluid Dynamics, Academic Press, 1982, pp. 273–285, chapter.

[23] C.R. Kharangate, H. Lee, I. Mudawar, Computational modeling of turbulent evaporating falling films, Int. J. Heat Mass Tran. 81 (2015) 52–62, https://doi.org/10.1016/j.ijheatmasstransfer.2014.09.068.

[24] T. Höhne, C. Vallée, Experiments and numerical simulations of horizontal two-phase flow regimes using an interfacial area density model, J. Comput. Multiph. Flows 2 (2010) 131–143, https://doi.org/10.1260/1757-482x.2.3.131.

[25] R. Denèfle, S. Mimouni, J.-P. Caltagirone, S. Vincent, Multifield hybrid approach for two-phase flow modeling – Part 1: adiabatic flows, Comput. Fluid 113 (2015) 106–111, https://doi.org/10.1016/j.compfluid.2014.07.018.

[26] H.J. Zhu, Y.H. Lin, L.H. Xie, FLUENT Fluid Analysis and Simulation Practical Tutorial, People's Posts and Telecommunications Press, 2010.

[27] W.D. Pointer, Y. Liu, Eulerian two-fluid RANS-based CFD simulations of a helical coil steam generator boiling tube, in: 17th International Topical Meeting on Nuclear Reactor Thermal Hydraulics, vol. 2017, NURETH, 2017.

[28] F. Gauss, D. Lucas, E. Krepper, Grid studies for the simulation of resolved structures in an Eulerian two-fluid framework, Nucl. Eng. Des. 305 (2016) 371–377, https://doi.org/10.1016/j.nucengdes.2016.06.009.

[29] I. Perez-Raya, S.G. Kandlikar, Discretization and implementation of a sharp interface model for interfacial heat and mass transfer during bubble growth, Int. J. Heat Mass Tran. 116 (2018) 30–49, https://doi.org/10.1016/j.ijheatmasstransfer.2017.08.106.

[30] Y. Sato, B. Niceno, A sharp-interface phase change model for a mass-conservative interface tracking method, J. Comput. Phys. 249 (2013) 127–161, https://doi.org/10.1016/j.jcp.2013.04.035.

[31] Y. Sato, B. Niceno, Pool boiling simulation using an interface tracking method: from nucleate boiling to film boiling regime through critical heat flux, Int. J. Heat Mass Tran. 125 (2018) 876–890, https://doi.org/10.1016/j.ijheatmasstransfer.2018.04.131.

[32] A. Hillier, T. Van Doorsselaere, K. Karampelas, Estimating the energy dissipation from Kelvin–Helmholtz instability induced turbulence in oscillating coronal loops, Astrophys. J. Lett. 897 (2020) L13, https://doi.org/10.3847/2041-8213/ab9ca3.

[33] T. Yamada, T. Shigechi, S. Momoki, K. Kanemaru, An analysis of film boiling around a vertical finite-length cylinder. Reports of the Faculty of Engineering, Nagasaki University, 2001, pp. 1–11.

[34] D. Landek, J. Župan, T. Filetin, A prediction of quenching parameters using inverse analysis, Mater. Perform. Char. 3 (2014) 229–241, https://doi.org/10.1520/mpc20130109.

[35] C. Demirel, Experimentelle Untersuchung und Simulation des Abschreckprozesses von bauteilähnlichen Geometrien aus G-AlSi7Mg, Technische Universität, Berlin, 2009, https://doi.org/10.14279/depositonce-2228. PhD thesis.

[36] E. Troell, H. Kristoffersen, J. Bodin, S. Segerberg, I. Felde, Unique software bridges the gap between cooling curves and the result of hardening, HTM J. Heat Treat. Mate. 62 (2007) 110–115, https://doi.org/10.3139/105.100414.

[37] S. Momoki, T. Yamada, T. Shigechi, K. Kanemaru, T. Yamaguchi, Film boiling around a vertical cylinder with top and bottom horizontal surfaces, in: ASME/JSME 2007 Thermal Engineering Heat Transfer Summer Conference Collocated with the ASME 2007 InterPACK Conference, 2007, pp. 611–619, https://doi.org/10.1115/ht2007-32733.

[38] T. Yamada, T. Shigechi, S. Momoki, K. Kanemaru, T. Yamaguchi, Subcooled film boiling heat transfer around a vertical finite-length cylinder, Trans. Jpn. Soc. Mech. Eng. 73 (2007) 1715–1722, https://doi.org/10.1299/kikaib.73.1715. B.
[39] T. Yamada, T. Shigechi, S. Momoki, K. Kanemaru, T. Yamaguchi, Study on Subcooled Film Boiling Heat Transfer Around a Vertical Finite-Length Cylinder : 1st Report : Examination of Correlation Equations for Heat Transfer Reports of the Faculty of Engineering, 2005, pp. 1–10.
[40] T. Yamada, Study on Film Boiling Heat Transfer Around a Vertical Cylinder with Top and Bottom Horizontal Surfaces, Nagasaki University, 2007. PhD thesis, https://nagasaki-u.repo.nii.ac.jp/record/22671/files/paper080324.pdf.
[41] B. Halasz, A. Galović, I. Boras, Toplinske tablice. Fakultet Strojarstva I Brodogradnje, 2013. Zagreb.
[42] J.-C. Li, Y.-J. Wei, C. Wang, H.-Y. Deng, Water-entry cavity of heated spheres, Acta Phys. Sin. 65 (2016) 204703, https://doi.org/10.7498/aps.65.204703, 204703.
[43] v.D. Gerard, A Study on Mathematical Models for Turbulent Flows, WFW87.026, Technische Universiteit Eindhoven, Eindhoven, 1987. https://research.tue.nl/files/4318035/625334.pdf.